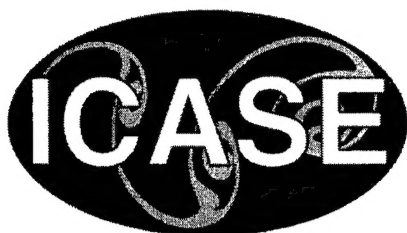NASA/CR-2000-210620
ICASE Report No. 2000-44

Optimization of Chemical Vapor Infiltration with Simultaneous Powder Formation

A. Ditkowski, D. Gottlieb, and B.W. Sheldon
Brown University, Providence, Rhode Island

ICASE
NASA Langley Research Center
Hampton, Virginia

Operated by Universities Space Research Association

DISTRIBUTION STATEMENT A
Approved for Public Release
Distribution Unlimited

National Aeronautics and
Space Administration

Langley Research Center
Hampton, Virginia 23681-2199

November 2000

20001214 014

OPTIMIZATION OF CHEMICAL VAPOR INFILTRATION WITH SIMULTANEOUS POWDER FORMATION*

A. DITKOWSKI[†], D. GOTTLIEB[‡], AND B.W. SHELDON[§]

Abstract. A key difficulty in isothermal, isobaric chemical vapor infiltration is the long processing times that are typically required. With this in mind, it is important to minimize infiltration times. This optimization problem is addressed here, using a relatively simple model for dilute gases. The results provide useful asymptotic expressions for the minimum time and corresponding conditions. These approximations are quantitatively accurate for most cases of interest, where relatively uniform infiltration is required. They also provide useful quantitative insight in cases where less uniformity is required. The effects of homogeneous nucleation were also investigated. This does not affect the governing equations for infiltration of a porous body, however, powder formation can restrict the range of permissible infiltration conditions. This was analyzed for the case of carbon infiltration from methane.

Key words. composites, chemical vapor deposition (CVD), optimization, computer simulation, theory

Subject classification. Physical Sciences

1. Introduction. A variety of materials are produced by infiltration processes. In these techniques a fluid phase (i.e., a gas or a liquid) is transported into a porous structure, where it then reacts to form a solid product. These methods are particularly important for producing composite materials, where the initial porous perform is composed of the reinforcement phase (i.e., fibers, whiskers, or particles) and infiltration produces the matrix [1], [2]. A detailed assessment of the relevant reaction and mass transport rates during infiltration requires mathematical modeling, using a minimum of two coupled partial differential equations which describe changes in the reactant concentration and the solid structure as a function of both position and time. This type of modeling can also be extended to analyze the optimization and control of infiltration processes.

The research presented here specifically considers optimization for a set of two equations which describe isothermal, isobaric chemical vapor infiltration (CVI). In this process a vapor-phase precursor is transported into the porous preform, and a combination of gas and surface reactions leads to the deposition of the solid matrix phase. During infiltration the formation of the solid product phase eventually closes off porosity at the external surface of the body, blocking the flow of reactants and effectively ending the process. This is a key feature of most infiltration processes. Isothermal, isobaric CVI often requires extremely long times, so it is generally important to minimize the total processing times.

This paper considers the problem of determining the optimal pressure and temperature which correspond to the minimum infiltration time. From a practical perspective, the nature of the porous preform is often predetermined by the intended application (e.g., the physical dimensions and the fiber size are invariants). Thus, the process can only be controlled with process variables: temperature, pressure, and gas composition.

[†]Division of Applied Mathematics, Brown University, Providence, RI 02912

[‡]Division of Applied Mathematics, Brown University, Providence, RI 02912. This research was supported by the National Aeronautics and Space Administration under NASA Contract No. NAS1-97046 while the second author was in residence at ICASE, NASA Langley Research Center, Hampton, VA 23681-2199.

[§]Division of Engineering, Brown University, Providence, RI 02912

Note that the pressure and temperature determine several different physical quantities in the model, such that the general understanding of the optimum conditions is not immediately obvious from the basic formulation.

Several previous efforts have addressed minimal infiltration times [7], [8], [9], [10], [11]. The work described here differs from these previous efforts in several ways. First, the asymptotic solutions obtained here make it possible to estimate the optimal conditions without conducting detailed numerical calculations. This paper uses a relatively simple mathematical model which is based on the diffusion and reaction of a single, dilute precursor. However, the numerical results which are used to verify and understand the limitations of the asymptotic results are generally similar to previously reported numerical results. Also, the results presented here are based on carbon CVI from methane, in comparison with previous efforts on CVI optimization which have emphasized SiC CVI from methyltrichlorosilane. The use of different chemistry does not change the general conclusions obtained here, however, the actual values do correspond to a somewhat different process. This paper also considers an additional constraint due to homogeneous nucleation (powder formation), which has not been treated in previous efforts. Powder formation can be significant in many CVI processes (including carbon formation), and this effect can alter the optimal temperature and pressure under certain conditions.

This paper is organized as follows: Section 2 presents the basic set of two partial differential equations used to model isothermal, isobaric CVI (including initial and boundary conditions). A definition for a successful process and a discussion on the optimization problem is given. In Section 3 an analysis of the optimization problem is given. The analysis performed is based on asymptotic expansions as well as computations. The results of the analysis are optimal working pressure and temperature. In Section 4 the effects of powder formation in the analysis are included in the analysis; here too the pressure and temperature to minimize the final time are provided. In Section 5 a discussion of the significance of these results is presented.

2. Formulation. A mathematical description of infiltration requires one or more partial differential equations which describe the evolution of the matrix (i.e., the solid phase), and one additional partial differential equation for each chemical species in the fluid phase. For a simple pore structure, the continuity equation for species i is

$$(2.1) \qquad \frac{\partial(\varepsilon C_i)}{\partial t} + \nabla \cdot N_i = \sum_{r}^{n_r} \nu_{ir} R_r$$

where t is time, ε is the void fraction of the media, C_i nd N_i are the concentration and the flux of species i, n_r is the number of the gaseous species, ν_{ir} is the stoichiometric coefficients for the ith gaseous species in the rth reaction, and R_r represents the volumetric reaction rate of reaction r.

The basic partial differential equation(s) which describe reaction and mass-transport in porous media (i.e., the fluid phase) are well-established [3], [5]. For example, the Dusty-Gas model [6] is typically used to describe multicomponent diffusion and convection in a porous body.

$$(2.2) \qquad \frac{N_i}{D_{K_i}} + \frac{RT}{P} \sum_{j \neq i} \frac{C_j N_i - C_i N_j}{\mathcal{D}_{M_{ij}}} = -\nabla C_i - \frac{C_i B_e}{\mu D_{K_i}} \nabla P$$

The simplest formulation for the fluid phase is obtained by considering one reacting species. For highly diluted reactant systems, the Dusty-Gas model can be simplified to give the following approximate expression for the flux in one spatial dimension (Z):

$$(2.3) \qquad N = -D \frac{\partial C}{\partial Z}$$

where C is the concentration of the diluted species and Z is the distance into the preform. It is convenient to write C in terms of the temperature T, the total pressure, P, and the mole fraction of the reacting species, X:

$$(2.4) \qquad C = \frac{XP}{RT}.$$

For a diffusion-limited process, with one dilute reactant species in one spatial dimension, Eq. (2.1) becomes (using Eq. (2.3) and Eq. (2.4)):

$$(2.5) \qquad \frac{\partial(\varepsilon X P)}{\partial t} = \frac{\partial}{\partial Z}\left[D \frac{\partial x P}{\partial Z} \right] - \frac{u S_v(\varepsilon)}{V_M}$$

where V_M is the molar volume of the solid product , u is the rate at which the solid product grows (volume/area/time) and $S_v(\varepsilon)$ is the gas/solid surface area per unit volume of the porous solid. The last term in Eq. (2.5) describes the rate at which the gas-phase precursor is consumed (or created) by chemical reactions inside of the pores, with the assumption that there are no homogeneous gas-phase reactions.

Describing the evolution of the matrix phase is equivalent to considering the change in the void fraction, ε (i.e., the volume fraction of gas inside of the porous solid). The evolution of ε is given by:

$$(2.6) \qquad \frac{\partial \varepsilon}{\partial t} = -u S_v(\varepsilon).$$

The boundary conditions most often used for CVI models are to fix the concentration at the outer surface of the preform, and to assume that diffusion occurs in from two opposite sides, such that there is no net flux in the middle of the preform (i.e., at $Z = L$, where L is the half-thickness of the preform):

$$(2.7) \qquad X(0,t) = X_o$$

$$(2.8) \qquad X_z(1,t) = 0$$

where $z = Z/L$.
The initial condition is given by:

$$(2.9) \qquad \varepsilon(z,0) = \varepsilon_0(z).$$

A specific CVI model requires expressions for u, S_v, and D. Our objective in this work is to use relatively simple formulations for each, as a basis for assessing optimization during isothermal, isobaric CVI. As an example, consider the formation of carbon matrix composites from a mixture of CH_4 in an H_2 carrier gas, where the following net reaction occurs:

$$(2.10) \qquad CH_4 \text{ (g)} \xrightarrow{H_2} C(s) + 2\ H_2(g).$$

The form of Eq. (2.5) is based on the assumption that the CH_4 concentration, C, is dilute (i.e., the reactant concentration is much smaller than the carrier gas concentration). If the carbon growth rate is proportional to the precursor concentration, then:

3

$$(2.11) \qquad u = k\frac{xP}{RT}$$

where k is the reaction rate constant (with units $\frac{1}{time}$) and R is the gas constant. The standard Arrhenius expression for k is:

$$(2.12) \qquad k = A_k \exp(-Q/T)$$

where Q is the activation energy divided by the R and A_k is a pre-exponential factor.

The preforms used for CVI typically have a complex porous structure. However, a cylindrical pore is often used to formulate simple models. This leads to the following expression for S_v:

$$(2.13) \qquad S_v(\varepsilon) = \frac{2\sqrt{\varepsilon_o}\sqrt{\varepsilon}}{r_0}$$

where r_0 is the initial pore radius and ε_o is the initial concentration of ε.

The effective diffusivity of the dilute species, D, can be expressed as

$$(2.14) \qquad D = \frac{\varepsilon}{\theta}D_M\left[1 + N_k(\varepsilon)\right]^{-1}$$

$$D_M = \frac{A_M T^{3/2}}{P}$$

where D_M is the binary diffusion coefficient for the reactant species in the carrier gas (e.g., CH_4 in H_2), A_M is a species dependent constant, N_k is the ratio of D_M and the Knudsen diffusion coefficient, and θ is the tortuosity factor. For randomly distributed cylindrical pores, θ is estimated to be 3, and N_k is given by:

$$N_k = \frac{A_D T}{\eta^{1/2} P}$$

where

$$(2.15) \qquad A_D = \frac{A_M \eta_0 T^{*1/2}}{D_K^0 P}$$

D_K^0 is the Knudsen diffusion coefficient for the initial pore size, at some reference temperature T^*.

Substituting Eqs. (2.11) and (2.13) into Eqs. (2.6) and (2.5) gives the following forms:

$$(2.16) \qquad \frac{\partial \eta(z,t)}{\partial t} = -\frac{\beta}{2}c(z,t)$$

$$(2.17) \qquad \frac{\partial}{\partial z}\left(f(\eta(z,t))\frac{\partial c(z,t)}{\partial z}\right) = \alpha^2\, \eta(z,t)c(z,t)$$

4

TABLE 2.1

Values of the constants.

A_α	$6.35\,(10)^{21}$ K$^{3/2}$ atm^{-1}
A_β	$3.64\,(10)^{18}$ K$^{3/2}$ atm^{-1} sec^{-1}
$\eta_0 = \sqrt{\epsilon(t=0)}$	0.85
Q	55000 K [17]
A_D: $10_{\mu m}$ diam fibers	$1.54\,(10)^{-5}$ atm/K
$80_{\mu m}$ diam fibers	$1.93\,(10)^{-6}$ atm/K
$200_{\mu m}$ diam fibers	$7.7\,(10)^{-7}$ atm/K

where

$$(2.18) \qquad f(\eta) = \frac{P\eta^3}{3(P\eta + A_D T)}$$

$$(2.19) \qquad \eta = \sqrt{\varepsilon}$$

$$(2.20) \qquad \alpha^2 = A_\alpha \frac{P e^{(-Q/T)}}{T^{3/2}}$$

$$(2.21) \qquad \beta = A_\beta \frac{X_0 P e^{(-Q/T)}}{T}$$

$$(2.22) \qquad A_\alpha = \frac{2 A_k \sqrt{\varepsilon_o} L^2}{V_M r_0 A_M R}$$

$$(2.23) \qquad A_\beta = \frac{2 A_k \sqrt{\varepsilon_0}}{r_0 R}$$

Where r_0 is the initial pore radius and X_0 denotes the fraction of the active gas in the inlet (at $z = 0$). Note that α^2 is dimensionless and that β has units of inverse time. The time derivative in Eq. (2.5) has been removed in Eq. (2.17), which is permissible because a pseudo-steady state C profile is achieved in a short amount of time (i.e., compared to the time scale over which ε changes) [4]. Transforming ε to η simplifies equation (2.16). Note that η is proportional to S_v, so η can be viewed as a dimensionless surface area per volume. Values of the constants in Eqs.(2.18)-(2.23) are given in Table 2.1, for the case of carbon CVI from methane, (see Eq.(2.10)), with a preform thickness of $2L = 3$mm.

The system (2.16), (2.17) is subject to the initial condition

$$(2.24) \qquad \eta(z,0) = \eta_0(z).$$

This paper treats only the case of a uniform initial condition, $\eta_0(z) = \eta_0$. The boundary conditions are (see (2.7), (2.8)):

$$(2.25) \qquad c(0,t) = 1$$

$$(2.26) \qquad \frac{\partial c}{\partial z}\Big|_{z=1} = 0.$$

With this model it can be shown that:

- The value of the void function in the inlet $z = 0$, is

$$(2.27) \qquad \eta(0,t) = \eta_0 - \frac{\beta}{2}t$$

5

- There exists a critical time $t_c = \frac{2\eta_0}{\beta}$. At this time, the void function vanishes at $z = 0$, the inlet closes completely, and the process ends.
- The void function η and the concentration function c are bounded from above and below. $0 < c(z, t) \leq 1$, $\eta(0, t) \leq \eta(z, t) \leq \eta_0$ for $t < t_c = \frac{2\eta_0}{\beta}$.
- For any time $t < t_c$, the void function $\eta(z, t)$ is monotonically increasing function of the spatial variable z.
- The concentration function $c(z, t)$ is monotonically decreasing function of the spatial variable z.

The literature on diffusion and reaction in porous media typically uses a dimensionless ratio of the diffusion and reaction rates, sometimes known as the Thiele modulus. This parameter varies during infiltration, because of changes in the microstructure with time. Thus, previous CVI modeling has used an initial Thiele modulus as an approximate assessment of the relative infiltration kinetics [4], [7], [8]. In terms of the formulation specified here, the initial Thiele modulus is equal to $\alpha^2 \eta(z, 0)/f(\eta(z, 0))$. In general, when α^2 is small, diffusion is fast and infiltration is relatively uniform. When α^2 is large, the deposition reaction is fast and infiltration is highly non-uniform.

The parameters α^2 and β depend on the three key process variables: T, P, and X_0. Process optimization during CVI is achieved by setting these variables to optimal values. In isothermal, isobaric CVI the infiltration kinetics are controlled by diffusion and the deposition reaction. To achieve relatively uniform infiltration, diffusion must be fast relative to the deposition rate. This is typically accomplished by choosing processing conditions that result in a slow deposition rate, which usually leads to long infiltration times. Thus, the primary basis for process optimization is to obtain the desired amount of infiltration in the shortest possible time.

A general definition of a successful process includes two considerations:

1. At the end of the process (at time $t = t_f$) the void function $\eta(z, t_f)$ should be a small fraction of its initial value, either in the whole interval or in a certain portion of the interval $0 \leq z \leq z_1$.
2. For the process to yield good results it is important that the void function is <u>uniformly</u> small along the z axis.

Mathematically, we express these considerations by stating that a process is successful if for some time t_f

(2.28) $$\eta(z_1, t_f) \leq k_1 \eta_0$$

(2.29) $$\eta(0, t_f) = k_0 \eta_0$$

$k_0 << 1$, $k_0 < k_1$. Equation (2.28) states that the final values of the void function η should be small in the interval between the inlet and the point z_1 (note that $\eta(z, t)$ is monotonically increasing function of the spatial coordinate z). In most problems of interest $z_1 = 1$. Conditions (2.28) and (2.29) state that the void function should be uniformly small. Also, from (2.27), (2.29), the final time, t_f, is given by:

(2.30) $$t_f = (1 - k_0)\eta_0 \frac{2}{\beta}.$$

Note that the time for the process to end decreases as a function of β (itself a function of the temperature and pressure, given in (2.21)).

The goal of the analysis in the following sections is to find the temperature and pressure that minimize the final time t_f for achieving a successful process.

6

3. Analysis of the Optimization Problem. Evaluation of Eq. (2.27) requires an approximation for $\eta(z_1, t_f)$ in terms of the pressure and temperature. There are two ways to obtain it: either by asymptotic expansions or by direct numerical solution of the system (2.16),(2.17).

3.1. Asymptotic Expansions. The set of equations (2.16), (2.17) is nonlinear and explicit solutions can not be obtained. However some analytical approximation may be derived by noting that in most of the problems of interest α^2 is small, and therefore it makes sense to expand the solutions in power of α^2. The details of obtaining this expansion to order α^2 will be given elsewhere [16]. For small α^2 the final result is:

$$(3.1) \qquad c(z, t) \sim 1 - \alpha^2(z - z^2/2)\frac{f(E)}{E}$$

$$(3.2) \qquad \eta(z, t) \sim E(t) + 3\alpha^2(z - z^2/2)\left[\log\left(\frac{\eta_0}{E(t)}\right) + \frac{A_D T}{P}\left(\frac{1}{E} - \frac{1}{\eta_0}\right)\right]$$

Where

$$(3.3) \qquad E(t) = \eta_0 - \frac{\beta}{2}t$$

It can be shown that the error in the expansion is proportional to $\left(\frac{\alpha^2}{k_0}\right)^2$, where k_0 is the ratio between the final void function at the inlet and its initial value, as defined in (2.29). In the next subsection the numerical results and the asymptotic expansions are compared, to demonstrate the validity of the expansions in the range of relevant α^2.

The asymptotic expansion (3.2) is used to get an explicit form for the uniformity constraint (2.28) in terms of the temperature T and the pressure P. Substituting (3.2) into (2.28) gives:

$$(3.4) \qquad k_0\eta_0 + 3\alpha^2(z_1 - z_1^2/2)\left[\log\left(\frac{1}{k_0}\right) + \frac{A_D T}{P\eta_0}\left(\frac{1}{k_0} - 1\right)\right] \leq k_1\eta_0$$

Substituting α^2 from (2.20) and rearranging gives:

$$(3.5) \qquad J(P, T) \leq (k_1 - k_0)\eta_0.$$

where

$$(3.6) \qquad J(P, T) = 3A_\alpha\frac{P}{T^{3/2}}e^{-Q/T}(z_1 - z_1^2/2)\left[\log\left(\frac{1}{k_0}\right) + \frac{A_D T}{P\eta_0}\left(\frac{1}{k_0} - 1\right)\right]$$

Rearranging terms shows that uniformity is assured if

$$(3.7) \qquad P \leq \frac{B_0}{B_2}T^{3/2}e^{Q/T} - \frac{B_0}{B_2}T,$$

where

$$(3.8) \qquad B_0 = \frac{\eta_0(k_1 - k_0)}{A_\alpha 3(z_1 - z_1^2/2)}$$

$$(3.9) \qquad B_1 = \frac{A_D}{\eta_0}(\frac{1}{k_0} - 1)$$

$$(3.10) \qquad B_2 = \log(\frac{1}{k_0}).$$

These results can now be used to approximate the temperature and pressure that minimize the infiltration time. Recall (see (2.30)) that the final time t_f is inversely proportional to β given in (2.21). The final time t_f is therefore minimized if the function

7

$$(3.11) \qquad F(P,T) = \frac{P}{T} e^{-Q/T}$$

is maximized under the uniformity constraint (2.29). Inspection of (3.11) shows that in order to maximize β we have to take the equality sign in (3.7). Substituting this into (3.11), it is easily verified that the following function must be maximized:

$$(3.12) \qquad G(T) = \frac{B_0}{B_2} T^{1/2} - \frac{B_1}{B_2} e^{-Q/T}$$

This indicates that the final time t_f to achieve a successful process is minimized by choosing temperature and pressure satisfying

$$(3.13) \qquad T^{3/2} e^{Q/T} = \frac{B_1 Q}{B_0}$$

$$(3.14) \qquad P = \frac{B_1}{B_2}(Q - T).$$

Moreover the minimal final time t_f^{min} is given by

$$(3.15) \qquad t_f^{min} = \frac{2(1-k_0)\log(1/k_0)}{k_1 - k_0} \frac{A_\alpha Q}{A_\beta X_0} 3(z_1 - z_1^2/2) \frac{1}{T^{1/2}(Q-T)}$$

Where the temperature T is given by (3.13).

The explicit formulas (3.13)-(3.15) lead to the following observations:

1. The minimum final time, t_f^{min}, decreases as A_D decreases. (For example, as the molecular diffusion becomes dominant.)
2. t_f^{min} decreases as k_1 increases. This reflects the fact that increasing k_1 relaxes the uniformity condition.
3. As z_1 increases toward $z_1 = 1$, the minimum final time t_f^{min} increases.

3.2. Computational Results. In the previous subsection the asymptotic expansion of η was used to define a functional $J(P,T)$ such that each pair P, T that satisfies $J(P,T) \leq (k_1 - k_0)\,\eta_0$ leads to a solution that satisfies the conditions for a successful process, (2.28), (2.29). The optimal P and T was then obtained based on the final time. This result is approximately correct since the asymptotic expansion was used to approximate condition (2.28). This section uses numerical solutions of (2.16), (2.17) to create a 'numerical J functional', (i.e., a functional relation between P and T that ensures a successful process).

Two algorithms were used to solve this problem: one based on a finite difference approximation and one on spectral methods. These are described in the Appendix. The schemes were run with $k_0 = 0.1$, $z_1 = 1$ and $k_1 = 0.15$ or 0.7. Note that $k_1 = .15$ corresponds to relatively uniform infiltration while $k_1 = .7$ is relatively non-uniform. Although most applications require relatively uniform infiltration (i.e., lower k_1), there are some cases where a non-uniform profile may be desirable. Two reasons for a higher k_1 are that it enables faster infiltration times, and it produces materials with lower density. For example, both of these attributes are desirable during the formation of thin carbon-carbon composites for bipolar plates in proton exchange membrane (PEM) fuel cells [18].

Three values were taken for A_D, $1.54\,(10)^{-5}$, $1.93\,(10)^{-6}$ and $7.7\,(10)^{-7}$ (see Table 2.1). Plots of the numerical and the asymptotic J curves are presented in Figure 3.1, plots of t_f vs. P are presented in Figure 3.2.
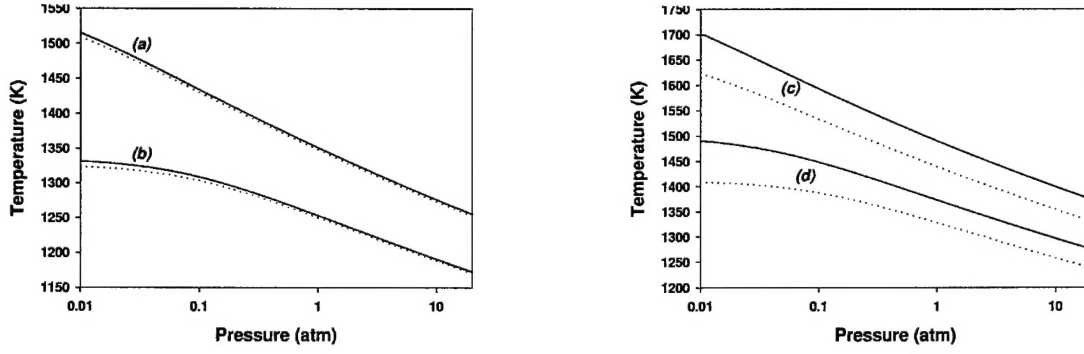
FIG. 3.1. *J-Curves obtained both numerically (solid lines) and by asymptotic analysis (dotted lines). Conditions on or below these lines will satisfy the uniformity condition (Eq. (3.35)). Conditions above this line do not satisfy the uniformity condition. All cases here correspond to $X_0 = 0.1$, with: (a) $k_1 = 0.15$, $10\mu m$ diameter fibers; (b) $k_1 = 0.15$, $200\mu m$ diameter fibers; (c) $k_1 = 0.7$, $10\mu m$ diameter fibers; (d) $k_1 = 0.7$, $200\mu m$ diameter fibers.*
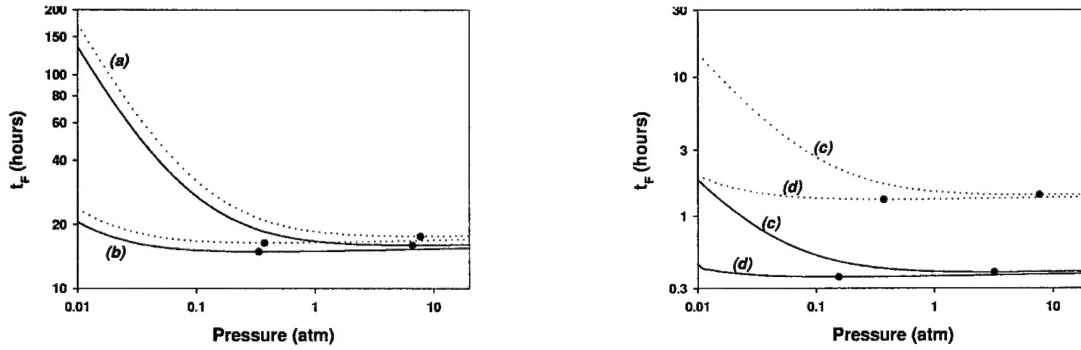

FIG. 3.2. *Times which correspond to conditions on the J-curves in Figure 3.1, with values obtained both numerically (solid lines) and by asymptotic analysis (dotted lines). The filled circles show the minimal time. (a) $k_1 = 0.15$, $10\mu m$ diameter fibers; (b) $k_1 = 0.15$, $200\mu m$ diameter fibers; (c) $k_1 = 0.7$, $10\mu m$ diameter fibers; (d) $k_1 = 0.7$, $200\mu m$ diameter fibers.*

The process is very sensitive to changes in the temperature T, as can be seen, for example, by comparing the results for $P = .1_{atm}$, $T = 1387\,K$, vs. $P = .1_{atm}$, $T = 1448\,K$ (for $k_1 = 0.7$ and $A_D = 1.54\,(10)^{-5}$). Increasing temperature by 61 degrees, ($\sim 4\%$), decreases the final time from 160.3_{min} to 31.4_{min}, i.e., by a factor of 5 and produces an infiltration profile which is much less uniform. This occurs because of the strong temperature dependence of the deposition reaction. As the fibers size increases t_f decreases slightly and the minimal time occurs at lower pressures.

When the uniformity requirement dictates that $k_1 = .15$ in (2.28), the condition $J(P,T) = (k_1 - k_0)\eta_0$ yields a P and T pair such that $\alpha^2 \sim .01$. In this case, the asymptotic expansions agree well with the numerical results. The predicted temperature that assures uniformity differs by only few degrees from the one obtained numerically, and t_f differs by less than 10%. When k_1 was increased to 0.7, The large value of α^2, (~ 0.1) leads to more inaccuracy in t_f, (See Table 3.1). However, the optimal temperatures predicted by the asymptotic result is still accurate within 10%.

9

TABLE 3.1
t_f for the optimal P and T.

A_D	k_1	Numerics			Asymptotics		
		P [atm]	T [K]	t_f [H]	P [atm]	T [K]	t_f [H]
$1.54\,(10)^{-5}$	0.15	6.605	1201.65	16.03	7.694	1195.06	17.62
$1.93\,(10)^{-6}$	0.15	0.830	1258.48	15.27	0.962	1251.37	16.80
$7.7\,(10)^{-7}$	0.15	0.334	1389.75	14.93	0.373	1282.43	16.42
$1.54\,(10)^{-5}$	0.7	3.185	1338.99	0.3934	7.694	1265.75	1.428
$1.93\,(10)^{-6}$	0.7	0.375	1492.76	0.3727	0.962	1405.28	1.357
$7.7\,(10)^{-7}$	0.7	0.155	1573.00	0.3632	0.373	1478.51	1.324

In all cases, the asymptotic results agree qualitatively with the numerical results. The curves obtained numerically were almost parallel to the asymptotic, and the points of minima are almost in the same place. The asymptotic results are conservative, they always overestimated the final time, and gave more restrictive conditions on P and T for uniformity. i.e., P and T obtained by the asymptotic analysis never predict a successful process if it does not exist. However, since P and T obtained by the asymptotic analysis may be much different from the optimal ones (obtained by the numerical analysis), t_f may be much larger then the minimal value (See Table 3.1).

4. Homogeneous Nucleation. CVI processes can be limited by homogeneous nucleation (i.e., powder formation) in the gas phase. This effect has not been treated in previous CVI models because it generally occurs outside of the solid preform. However, powder formation can impose serious limitations on CVI operating conditions during the formation of carbon and oxide matrices. Thus, this phenomena imposes a constraint on the allowable CVI operating conditions. Nucleation kinetics are typically described with:

$$(4.1) \qquad I = Z_I J^* A^* (X_0 P/RT) \exp(-\Delta g^*/k_B T)$$

where I is the steady-state nucleation rate, A^* is the area of a critical cluster, J^* is the flux at which atoms are added to a critical cluster, Δg^* is the free energy barrier to forming a critical cluster, k_B is Boltzmann's constant, and Z_I is the so-called Zeldovich factor, see [12]. A rigorous model requires that Z_I be evaluated numerically, however, using standard approximations for Z_I, the pre-exponential terms in (4.1) can be combined to give:

$$(4.2) \qquad I \cong (X_0 P/RT)^2 2(\gamma/k_B T)^{1/2} A_k \exp(-Q/RT) \exp(-\Delta g^*/kT)$$

where γ is the surface free energy of the cluster, and the constants A_k and Q describe the reaction rate constant (see (2.12)). In practice, the permissible value of I depends on the reactor configuration, as well as its actual value. For the current analysis, we assume that powder formation limits CVI when the nucleation rate exceeds some allowable level, I_{lim}. With this in mind, Eq. (4.1) can be revised to yield:
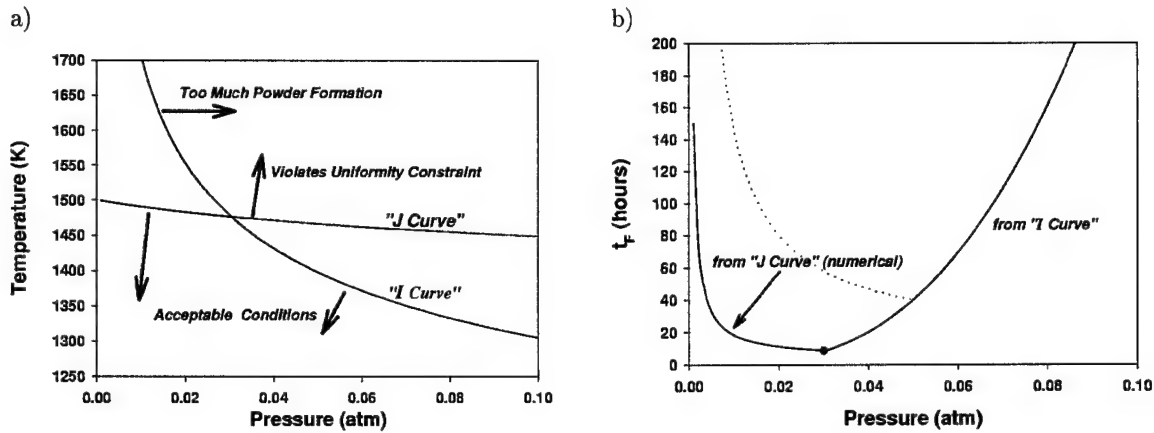
FIG. 4.1. *Effect of homogeneous nucleation for $k_1 = 0.7$, $X_0 = 0.01$, 10μm diameter fibers. (a) The numerically obtained J-Curve (uniformity constraint, Eq. (3.5)) and the I-curve (nucleation limit, Eq. (4.3) with $A_{\lim} = 2.0\,10^{21}$). (b) Limiting time as a function of pressure. The left part of the curve is determined by the numerically obtained J-curve and the right side is determined by the I-curve, with the minimal time shown by the filled circle. The dotted line corresponds to the approximate J-curve which was determined with asymptotics.*

$$(4.3) \qquad A_{lim} = I_{lim} k_B^{1/2}/A_k\gamma = (X_0 P)^2/T^{2.5}\exp(-A_I/T^m)$$

where the two exponential terms in Eq. (4.2) have been combined to give one term with two empirical constants, A_I and m. Since $\Delta g^\star$ can have a relatively complex T dependence, this empirical approach was adopted to provide a relatively simple expression. This form was applied to the results of Loll et al., who report threshold conditions for the onset of significant nucleation (i.e., X_0 vs. T at $P = 1_{\text{atm}}$) [13], [14]. A good fit to their experimental data was obtained with $m = 1.5$, $A_I = 750,000$ K^m, and $A_{lim} = 3.3\,(10)^{-17}$ atm^2/K$^{2.5}$. In general, the value of A_{lim} is somewhat arbitrary, since it reflects a threshold for a given reactor. By varying A_{lim}, it is possible to assess different tolerance levels for powder formation. For example, recent carbon CVI experiments at Oak Ridge National Laboratory tolerate higher powder formation levels than those described by Loll et al. with a threshold value that corresponds to $A_{lim} = 2.0\,(10)^{-21}$ atm^2/K$^{2.5}$ [15].

The effect of adding the powder formation constraint can be seen from Figure 4.1, where the I-curves are defined by Eq. (4.2). As seen in Figure 4.1a, the new constraint limits the pressures and temperatures to values which are below both the I and the J-curves. For a given pressure, the minimal t_f corresponds to a temperature on either the I or J-curve (whichever is lower). Thus if the minimal t_f found in Section 3 (i.e., when P and T are on the J-curves) to the left of the I-curve, then the additional constraint does not change the previous results. If, on the other hand, this point is on the right of the I-curve then, the minimal t_f occurs at the intersection between the I and J-curves. This point can be clearly seen as a cusp in the t_f vs. P in the right plot.

A complete assessment of X_0 effects requires solutions with the full Dusty-Gas model, because large values of X_0 violate the assumption of a dilute reactant gas. However, considering only values up to $X_0 = 0.1$ provides useful insight into optimizing dilute systems. Without the homogeneous nucleation constraint (i.e., as $A_{lim} \to \infty$), the minimal time is inversely proportional to X_0, and the optimal pressure and temperature do not vary with X_0 (see Section 3). However, homogeneous nucleation limits the operating conditions when
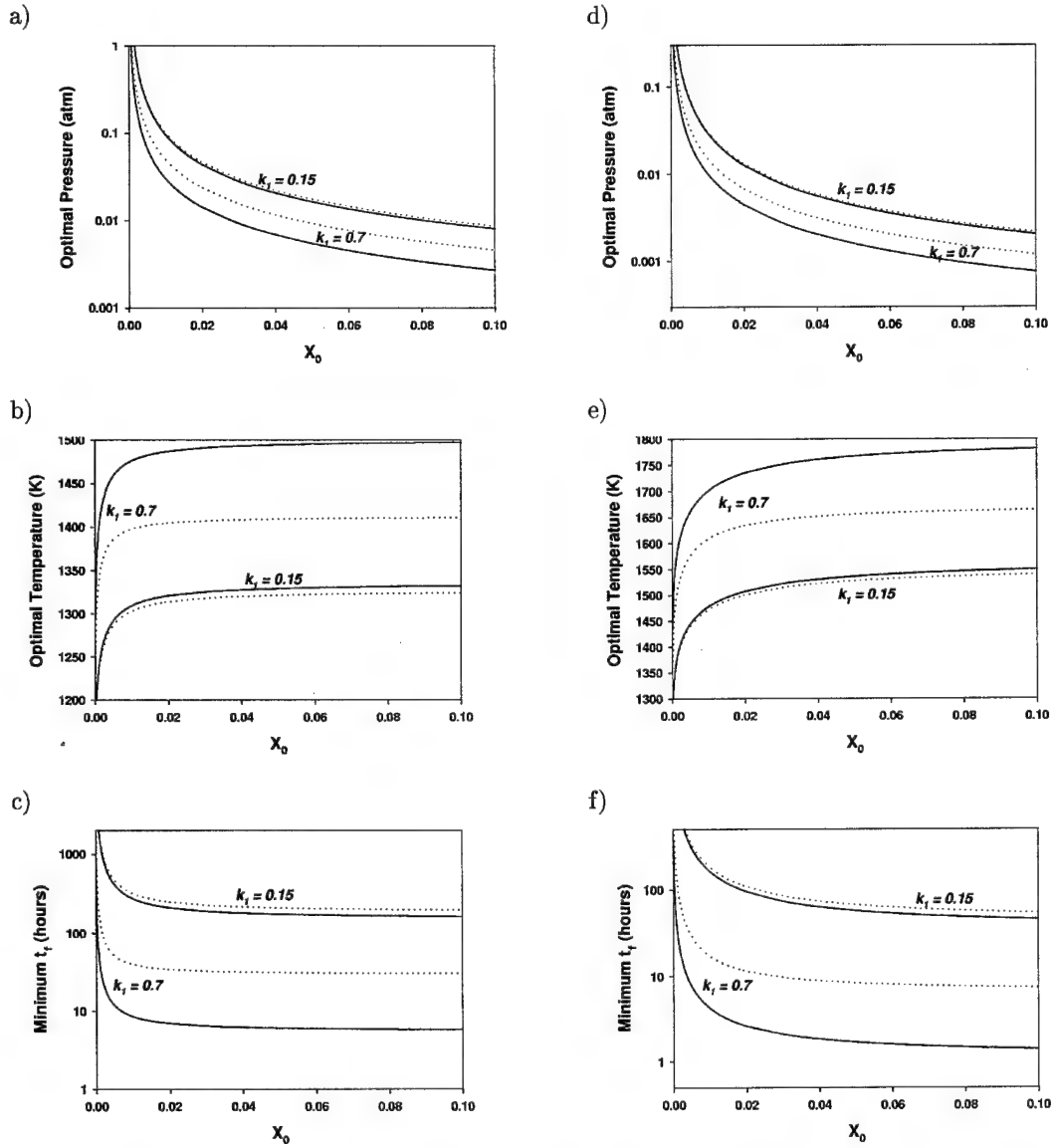
11

FIG. 4.2. *Effect of X_0 with $10\mu m$ diameter fibers: (a) optimal pressures; (b) optimal temperatures; (c) minimum infiltration times and with $200\mu m$ diameter fibers: (d) optimal pressures; (e) optimal temperatures; (f) minimum infiltration times.*

A_{lim} is low enough, as illustrated in Fig 3. The effect of this limitation on the optimal conditions and on the minimal time are shown in Figs. 4 and 5. These results lead to the following conclusions:

1. As in Section 3, the asymptotic results are in good agreement with the numerical results for $k_1 = .15$, where $\alpha^2 \sim .01$, and much less accurate in the case $k_1 = .7$ where $\alpha^2 \sim .1$. In both cases, however, the asymptotic results agree qualitatively with the numerical results.

2. Notwithstanding the dilute reactant gas restriction, t_f are monotonically decreasing functions of X_0, thus it is advisable to work in the 'highest' X_0 possible. However since the optimal P is also a monotonically decreasing functions of X_0, this value of X_0 is limited by the lowest operational
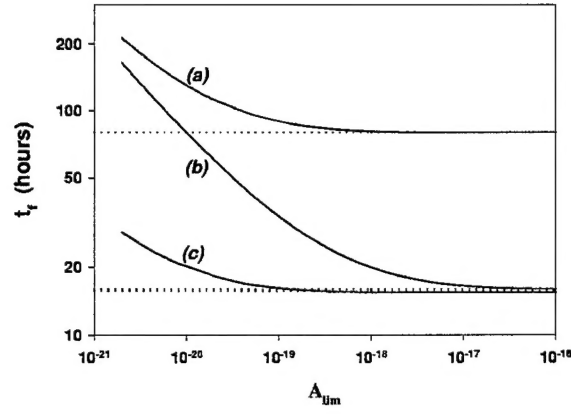
FIG. 4.3. *Effect of* Alim *on* t_f, *with* $k_1 = 0.15$: *(a)* 10μm *diameter fibers and* $X_0 = 0.1$; *(b)* 10μm *diameter fibers with* $X_0 = 0.02$; *(c)* 10μm *diameter fibers with* $X_0 = 0.1$. *All values are based on numerical results.*
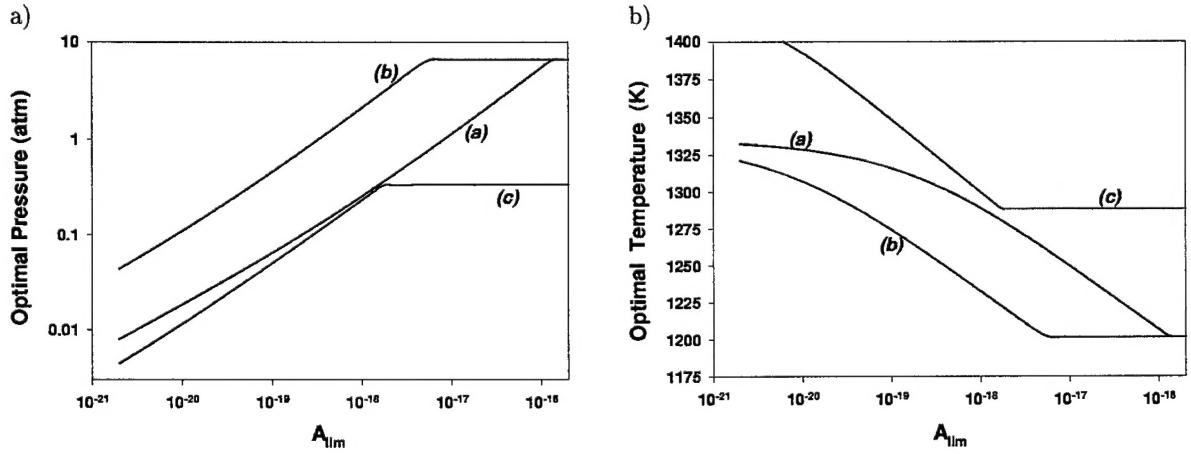

FIG. 4.4. *Effect of* $A_{\lim}$ *on the optimal pressure (a) and temperature (b), for the same cases plotted in Fig. 5.*

pressure. For example for working pressure of about 0.01_{atm}, the maximum allowable X_0 is only 0.05, for $200_{\mu m}$ diameter fibers $(A_D = 7.7\,(10)^{-7}\,\text{atm}\,\text{K}^{-1})$.

3. For a given X_0, as the fiber diameter increases, P and t_f decrease and T increases. But unlike Section 3, the differences here are significant. This occurs because the homogeneous nucleation condition forces us to work in a region where the dependence on A_D is much stronger.

4. The homogeneous nucleation constraint causes the optimal temperature and pressure to vary with X_0.

As the value of A_{lim} increases, the effects of homogeneous nucleation are less severe. This can be seen in Fig. 6, which shows the effects of varying I_{lim}. Note that the minimum infiltration time is dramatically increased when there is a significant limitation imposed by homogeneous nucleation. In general, the process must be operated at lower pressures to avoid powder formation. Some increase in the corresponding optimal temperature accompanies this decrease in pressure. The slope discontinuities in Fig. 6 correspond to the conditions where the homogeneous nucleation constraint no longer has an effect, (i.e., the optimal conditions are determined solely by the J curve).

5. Conclusions. Minimizing infiltration times for isothermal, isobaric CVI is important because processing times are typically very long. The work presented here provides a detailed assessment of the pressure and temperature which will minimize the total required time, based on a simplified model for a single, dilute reactant species. This formulation makes it possible to understand the basic physics of the problem in terms of a relatively small number of lumped parameters. The basic objective of this optimization problem is to obtain a density profile with a prescribed amount of uniformity, in the shortest possible time (Section 3). The asymptotic results are particularly useful, because they make it possible to determine optimal conditions without doing numerical calculations (under conditions where α^2 is small enough). Based on comparisons with the numerical results, the asymptotic forms are also qualitatively accurate when α^2 is larger. Thus, the asymptotic results provide a clear understanding of how the optimal conditions are related to the key parameters for the problem.

The effects of homogeneous nucleation were also analyzed, as an additional constraint on the basic optimization problem. This issue has not been considered in previous work on CVI modeling, however, it can limit operating conditions in systems were powder formation is significant (e.g., the formation of carbon matrix composites). The results obtained here provide a quantitative assessment of the conditions where homogeneous nucleation imposes limitations on infiltration conditions. When these limitations occur, powder formation also increases the minimum infiltration time.

6. Appendix. To gain confidence in our computations, two completely different numerical methods were used: the pseudospectral method and a finite difference method.

- In the pseudospectral Chebyshev method the grid points is chosen to be

$$(6.1) \qquad z_j = \frac{1 + \cos(\frac{\pi j}{N})}{2} \qquad 0 \leq j \leq N$$

where N is the total number of grid points and was 10 for most of the runnings.

The spectral differentiation matrix takes the value of a given function at the grid points z_j and yields the values of the derivative of the interpolation polynomial at these points. The points z_j are the nodes of the Gauss Lobatto Chebyshev quadrature formula. The matrix can be written explicitly:

$$(6.2) \qquad \begin{aligned} D_{jk} &= \frac{1}{2} \frac{c_j}{c_k} \frac{(-1)^{j+k}}{\sin \frac{\pi}{2N}(j+k) \sin \frac{\pi}{2N}(-j+k)} & j \neq k, \\ D_{jj} &= -\frac{1}{2} \frac{z_j}{\sin^2(\frac{\pi}{N} j)} & j \neq 0, N, \\ D_{00} &= -D_{NN} = \frac{2N^2 + 1}{6} \end{aligned}$$

We apply the matrix D_{jk} twice, once for the vector c taking into account the boundary condition $c(0, t) = 1$ and then to $f(\eta) c_z$ and taking into account that $c_z(1, t) = 0$. This yields a linear system for the values of $c(z_j, t)$.

In the next stage we update η by the standard third order Runge-Kutta scheme.

- A second-order finite-difference scheme using the equidistance grid

$$(6.3) \qquad z_j = \frac{j}{N} = jh \qquad 0 \leq j \leq N \ .$$

The differentiation matrix can be written explicitly:

$$
\begin{aligned}
D_{1\,1} &= -\tfrac{1}{h^2}\left(f(z_1 - h/2) + f(z_1 + h/2)\right) \\
D_{1\,2} &= \tfrac{1}{h^2} f(z_1 + h/2)
\end{aligned}
\qquad j = 1
$$

$$
\begin{aligned}
D_{j\,j-1} &= \tfrac{1}{h^2} f(z_j - h/2) \\
D_{j\,j} &= -\tfrac{1}{h^2}\left(f(z_j - h/2) + f(z_j h/2)\right) \\
D_{j\,j+1} &= \tfrac{1}{h^2} f(z_j + h/2)
\end{aligned}
\qquad j = 2 \dots N-1
$$

$$
\begin{aligned}
D_{N\,N-1} &= \tfrac{2}{h^2} f(1 - h/2) \\
D_{N\,N} &= -\tfrac{2}{h^2}\left(f(1 - h/2) + \alpha^2 \eta\right)
\end{aligned}
$$

f in the mid-points was interpolated. In each step we solve the system

$$
D\,\mathbf{c} = \begin{pmatrix} -\tfrac{1}{h^2} f(z_1 - h/2) \\ 0 \\ \vdots \\ 0 \end{pmatrix},
$$

In the next stage we use $\mathbf{c}$ to update η by the standard fourth order Runge-Kutta scheme. Since this scheme is less accurate we used 80 grid points.

The results of both schemes were compared and the differences in $\eta(z, t_f)$ were less then 10^{-6}.

REFERENCES

[1] E. FITZER AND R. GADOW, *Fiber-reinforced Silicon Carbide*, Am Ceram. Soc. Bull, **65** (1986), pp. 326-355.

[2] S.M. GUPTE AND J.A. TSAMOPOULOS, *Densification of Porous Materials by Chemical Vapor Infiltration*, J. Electrochem. Soc., **136** (1989), pp. 555-561.

[3] R. ARIS, *The Mathematical Theory of the Diffusion and Reaction in Permeable Catalysts*, Oxford University Press, London, 1975.

[4] H.-C. CHANG, *Minimizing Infiltration Time During Isothermal Chemical Vapor Infiltration*, Ph.D. Thesis, Brown University, 1995.

[5] F.A.L. DULLIEN, *Porous Media: Fluid Transport and Pore Structure*, Academic Press, New York, 1979.

[6] E.A. MASON AND A.P. MALINAUSKAS, *Gas Transport in Porous Media: The Dusty-gas Model*, Elsevier Science Publisher, 1983.

[7] B.W. SHELDON AND H.-C. CHANG, *Minimizing Densification Times During the Final Stage of Isothermal Chemical Vapor Infiltration*, Ceramic Transactions, B.W. Sheldon and S.C. Danforth, eds., American Ceramic Society, **42** (1994), pp. 81-93.

[8] H.-C. CHANG, T.F. MORSE, AND B.W. SHELDON, *Minimizing Infiltration Times During the Initial Stage of Isothermal Chemical Vapor Infiltration*, J. Mater. Proc. Manuf. Sci., **2** (1994), pp. 437-454.

[9] J.Y. OFORI AND S.V. SOTIRCHOS, *Optimal Pressures and Temperatures for Isobaric, Isothermal Chemical Vapor Infiltration*, AIChE Journal, **42** (1996), p. 2828.

[10] H.-C. CHANG, T.F. MORSE, AND B.W. SHELDON, *Minimizing Infiltration Times During Isothermal Chemical Vapor Infiltration with Chlorosilanes*, J. Am. Ceram. Soc., **7** (1997), pp. 1805-1811.

[11] H.-C. CHANG, D. GOTTLIEB, M. MARION, AND B.W. SHELDON, *Mathematical Analysis and Optimization of Infiltration Processes*, J. of Scientific Computing, **13** (1998), pp. 303-321.

[12] J. FEDER, K.C. RUSSELL, J. LOTHE, AND G.M. POUND, *Nucleation and Growth in Homogeneous Vapors*, Adv. Phys., **15** (1966), p. 111.

[13] P. LOLL, P. DELHAES, A. PACAULT, AND A. PIERRE, *Diagramme D'Existence et Properties de Composites Carbone-carbone*, Carbon, **13** (1975), p. 159.

[14] P. DELHAES, *CVD and CVI Processes of Carbon Materials*, Electrochemical Society Proceedings 97-25, M.D. Allendorf and C. Bernard, eds., Electrochemical Society, (1997), pp. 486-495.

[15] T.M. BESMANN, Oak Ridge National Laboratory, private communication, 1998.

[16] A. DITKOWSKI, D. GOTTLIEB, AND B.W. SHELDON, *On the Mathematical Analysis and Optimization of Chemical Vapor Infiltration in Materials Science*, M^{2}AN, **34**, No. 2 (2000), pp. 337-351.

[17] S. BAMMIDIPATI, G.D. STEWART, G.R. ELLIOTT, JR., S.A. GOKOGLU, AND M.J. PURDY, *Chemical Vapor Deposition of Carbon on Graphite by Methane Pyrolysis*, AIChE Journal, **42**, No. 11 (1996), pp. 3123-3132.

[18] T.M. BESMANN, J.W. KLETT, AND T.D. BURCHELL, *Carbon Composite for a PEM Fuel Cell Bipolarplate*, MRS Symposium Proceedings, Materials Research Society, Pittsburgh, Pennsylvania, (1998), pp. 365-370.